JACS
JOURNAL OF THE AMERICAN CHEMICAL SOCIETY
Article
pubs.acs.org/JACS

Understanding Polymorphism in Organic Semiconductor Thin Films through Nanoconfinement

Ying Diao,[†,‡,¶] Kristina M. Lenn,[§] Wen-Ya Lee,[†] Martin A. Blood-Forsythe,[∥] Jie Xu,[⊥] Yisha Mao,[†] Yeongin Kim,[†] Julia A. Reinspach,[†,‡] Steve Park,[†] Alán Aspuru-Guzik,[∥] Gi Xue,[⊥] Paulette Clancy,[§] Zhenan Bao,*[,†,¶] and Stefan C. B. Mannsfeld*[,‡,#]

[†]Department of Chemical Engineering, Stanford University, Stanford, California 94305, United States

[‡]Stanford Synchrotron Radiation Lightsource, [¶]Stanford Institute for Materials and Energy Sciences, SLAC National Accelerator Laboratory, 2575 Sand Hill Road, Menlo Park, California 94025, United States

[§]Department of Chemical Engineering, Cornell University, Ithaca, New York 14853, United States

[∥]Department of Chemistry and Chemical Biology, Harvard University, Cambridge, Massachusetts 02138, United States

[⊥]Department of Polymer Science and Engineering, Institute of Chemistry and Chemical Engineering, The State key Laboratory of Coordination Chemistry, The National Laboratory of Nanjing Microstructure Study, Nanjing University, Nanjing, 210093, PR China

[#]Center for Advancing Electronics Dresden, Dresden University of Technology, 01062 Dresden, Germany

Supporting Information

ABSTRACT: Understanding crystal polymorphism is a long-standing challenge relevant to many fields, such as pharmaceuticals, organic semiconductors, pigments, food, and explosives. Controlling polymorphism of organic semiconductors (OSCs) in thin films is particularly important given that such films form the active layer in most organic electronics devices and that dramatic changes in the electronic properties can be induced even by small changes in the molecular packing. However, there are very few polymorphic OSCs for which the structure−property relationships have been elucidated so far. The major challenges lie in the transient nature of metastable forms and the preparation of phase-pure, highly crystalline thin films for resolving the crystal structures and evaluating the charge transport properties. Here we demonstrate that the nanoconfinement effect combined with the flow-enhanced crystal engineering technique is a powerful and likely material-agnostic method to identify existing polymorphs in OSC materials and to prepare the individual pure forms in thin films at ambient conditions. With this method we prepared high quality crystal polymorphs and resolved crystal structures of 6,13-bis(triisopropylsilylethynyl)pentacene (TIPS-pentacene), including a new polymorph discovered via in situ grazing incidence X-ray diffraction and confirmed by molecular mechanic simulations. We further correlated molecular packing with charge transport properties using quantum chemical calculations and charge carrier mobility measurements. In addition, we applied our methodology to a [1]benzothieno[3,2-*b*][1]1benzothiophene (BTBT) derivative and successfully stabilized its metastable form.

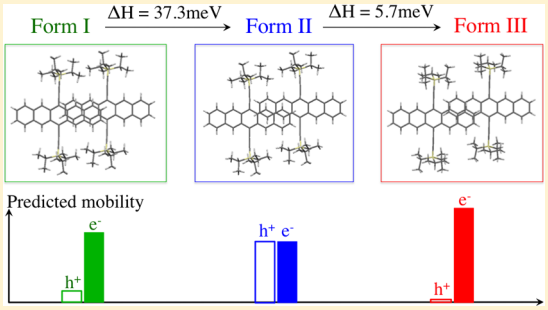

INTRODUCTION

Molecular packing has a profound impact on the solid-state properties of materials, including thermodynamic, kinetic, mechanical, electronic and optical properties. Since many organic compounds can pack into multiple distinct crystal structures (polymorphism), controlling polymorph formation is vital to a wide range of applications, e.g., pharmaceuticals, organic semiconductors, pigments, food, and explosives. Even though polymorphism of bulk crystals has been extensively studied, polymorphism in thin films is less understood and more difficult to control. There is hardly any approach reported to systematically identify and characterize polymorphism in thin films. In the context of organic semiconductors, this is especially important as charge transport occurs in the few layers of molecules near the dielectric interface, as opposed to in the bulk of the material. Moreover, a slight change in the π-orbital overlap between neighboring molecules in the thin films can lead to orders of magnitude difference in the charge carrier mobility through the active layer.[1,2] Such sensitivity of charge transport properties to thin film molecular packing makes polymorphism of OSCs a particularly interesting subject to study. Many benchmark OSCs have several polymorphs, such as copper phthalocyanine (CuPc),[3] poly(3-hexylthiophene) (P3HT),[4] 6,13-bis(triisopropylsilylethynyl)pentacene (TIPS-pentacene),[5] a-sexithiophene (6T),[6] pentacene,[7,8] rubrene,[9]

Received: July 15, 2014
Published: October 21, 2014

   dx.doi.org/10.1021/ja507179d | *J. Am. Chem. Soc.* 2014, 136, 17046−17057

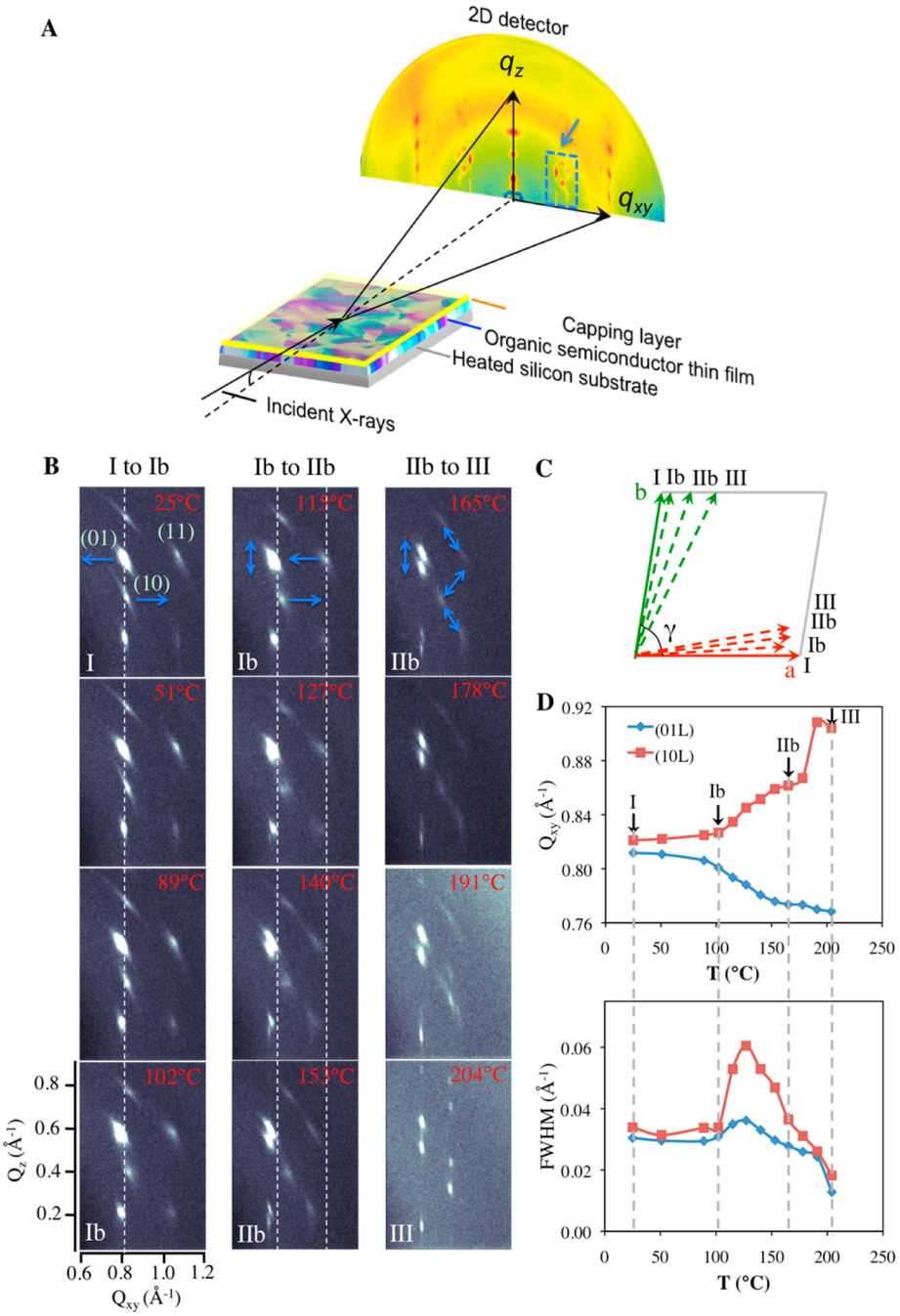

Figure 1. Phase space mapping of organic thin films via in situ grazing incidence X-ray diffraction (GIXD). (a) Schematic of the GIXD setup for in situ annealing. The area indicated by the blue dotted line and arrow corresponds to the image tiles shown in (b). (b) GIXD images during thermal annealing. Only the major reflections are shown. In the first diffraction image, the diffraction rods are labeled with their (hk) indexes. The blue arrows indicate the direction of peak shifts observed during each transition. The white dotted lines serve as guides to the eye for discerning peak shifts along Q_{xy}. The "2D powder" thin film was prepared via solution shearing from 30 mg/mL toluene solution at 50 °C with a shearing speed of 2 mm/s. From 25 to 102 °C (left column of (b)), the change is slight, with the (01) and (10) rods shifting in opposite directions. From 102 to 153 °C (middle column of (b)), substantial changes are observed in all three rods. Degenerate peaks in the (01) rod become separated in Q_z, and the (10) rod continues to shift to higher Q_{xy}. The (11) rod moves to lower Q_{xy} and at the same time the (−11) rod to higher Q_{xy} (not shown). These changes imply that the unit cell is becoming more oblique in-plane (γ deviating away from 90°) and that the tilting angle of the *c*-axis is varying. When heated further (b), a more abrupt polymorph transition is observed starting from approximately 165 °C and completing at around 200 °C. The diffraction pattern of the new phase has (10) and (11) rods merged to almost the same Q_{xy} position, indicating a γ close to 60° given similar lengths of the *a* and *b* axes. (c) Changes of the crystal unit cell during the polymorph transition, inferred from peak shifts in GIXD images. The inferred changes correspond well with the indexing results presented in Table S1. (d) Changes of in-plane peak positions (Q_{xy}) and peak widths (fwhm) of the two major reflections, (10) and (01), as a function of temperature.

2,8-difluoro-5,11-bis(triethylsilylethynyl)anthradithiophene (diF-TES-ADT),[10] 2,7-dioctyl[1]benzothieno[3,2-*b*][1] benzothiophene (C8-BTBT),[11] to name a few. With higher performing molecules being designed at an ever faster pace, controlled polymorph formation is becoming more and more important not only for tuning the charge transport properties,

dx.doi.org/10.1021/ja507179d | J. Am. Chem. Soc. 2014, 136, 17046−17057

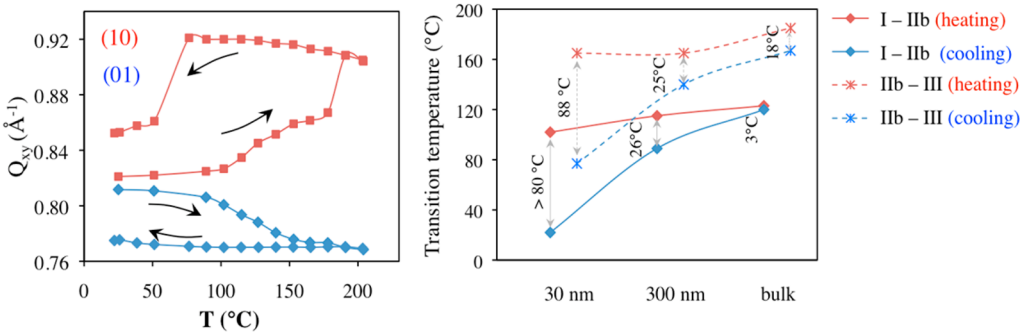

Figure 2. Transition temperature hysteresis and the effect of nanoconfinement. (left) Large transition temperature hysteresis observed during in situ annealing of a 30 nm thick film. The hysteresis is indicated from the Q_{xy} positions of (10) and (01) rods. The arrows point to the heating and cooling halves of the annealing cycle. (right) Effect of spatial confinement on the hysteresis of polymorph transition temperatures. The transition temperatures decrease with the decrease in characteristic dimensions. This effect is analogous to the melting point depression observed in confined systems.[24] Transition T of the bulk powder samples is obtained via DSC at a rate of 10 K/min (Figure S3). Note that the transition temperature shown in the image corresponding to I–IIb (cooling) in 30 nm films is not the actual one, but the upper bound. Therefore, the hysteresis is larger than 80 °C. The transition temperatures of thin films are approximate due to the large temperature stepping during annealing.

but also for producing "organic circuits" with consistent performance and high stability.

Controlling polymorphism in thin films of organic π-conjugated systems has been challenging. Commonly used approaches to control polymorphism, many of which developed for vapor-deposited pentacene, include the tuning of film thickness,[12,13] substrate reactivity, chemistry, and temperature,[14−16] the self-assembled monolayer (SAM) on which the OSC is deposited,[17] or the solvent used for postdeposition annealing.[18] Despite these advancements, it often takes years, even decades, to discover and resolve all the polymorphic structures of an OSC compound (e.g., close to 50 years in the case of pentacene). The challenge for controlling their polymorphism is manifold. First, different polymorphs of OSCs typically have closely matched cohesive energies and low kinetic barrier to solid−solid transformation. In other words, the free energy landscape of OSC crystals is relatively flat. This is due to the fact that their intermolecular interactions are characterized by nonselective van der Waals forces and electrostatic interactions. This characteristic often renders it difficult to isolate and stabilize metastable polymorphs. Recently, kinetic trapping has been utilized for accessing metastable polymorphs,[1,19] however, at the expense of much compromised film morphologies. For resolving the crystal structures and correlating with charge transport properties, it is necessary to obtain highly crystalline, ideally single-crystalline thin films, which is particularly challenging for metastable polymorphs. These obstacles severely hinder the understanding of the molecular origin and the rational control of polymorphism.

In this study, we show that nanoconfinement is an effective strategy for stabilizing the transient metastable forms at near ambient conditions. We further print phase-pure, high-quality crystalline thin films of metastable forms for resolving the crystal structures and correlating with charge transport properties, using the fluid-enhanced crystal engineering technique (FLUENCE) we recently developed.[2,20] First, we demonstrate this method using TIPS-pentacene, a benchmark and high-performing OSC molecule.[21] We mapped the structural phase space of TIPS-pentacene thin films using in situ Grazing Incidence X-ray Diffraction (GIXD) and molecular simulations. A new polymorph of this extensively studied molecule was found, which is metastable at room temperature. We observed enhanced kinetic stability of metastable polymorphs in confined thin films, manifested as enlarged hysteresis of polymorph transition temperatures. A thin film refinement technique that we developed was used to solve the thin-film structures. The result revealed a different side chain conformation and an extremely close $\pi-\pi$ stacking distance in the new polymorph. We also investigated the impact of molecular packing on the charge transport properties using a combination of experiments and quantum chemical calculations. Independently, discovery of polymorphs as particularly low-lying energetic forms of the structure and the molecular origin of this polymorphism of TIPS-pentacene are inferred from molecular mechanics calculations and structural refinement. To demonstrate the versatility of the above methodology, we revealed the thin film polymorphism for a [1]benzothieno-[3,2-*b*][1]1benzothiophene (BTBT) derivative, whose molecular packing adopts a herringbone motif, substantially different from the brick-wall packing of TIPS-pentacene.

RESULTS

Mapping the Phase Space via In Situ X-ray Diffraction. The most commonly used method for measuring the phase transition of bulk materials is differential scanning calorimetry (DSC). Using DSC, only one polymorph transition event was previously observed using TIPS-pentacene bulk powders (the second transition was overlooked due to low transition enthalpy).[5] Here we show that the full details of the phase space can be revealed using in situ X-ray diffraction during thermal annealing of the ultrathin films (referred to as "in situ annealing" experiments hereafter). Synchrotron X-ray diffraction is necessary to generate sufficient diffraction intensity from ultrathin films (i.e., 20−100 nm) with short exposure times (*i.e.*, 10−30s). Shown in Figure 1a, an in situ annealing "cell" was constructed by sandwiching the active layer (TIPS-pentacene) between the substrate (Si wafer) and a capping layer (see Experimental Methods). The capping layer was found to be essential. Otherwise sublimation of the active layer occurs during annealing. The in situ annealing results were found to be insensitive to the specific capping layer used. It is important to note that the ideal active layer should have the characteristics of a "2D powder", wherein the crystalline grains are randomly oriented in-plane but are highly oriented out-of-plane, so as to generate relatively well-defined diffraction

dx.doi.org/10.1021/ja507179d | J. Am. Chem. Soc. 2014, 136, 17046−17057

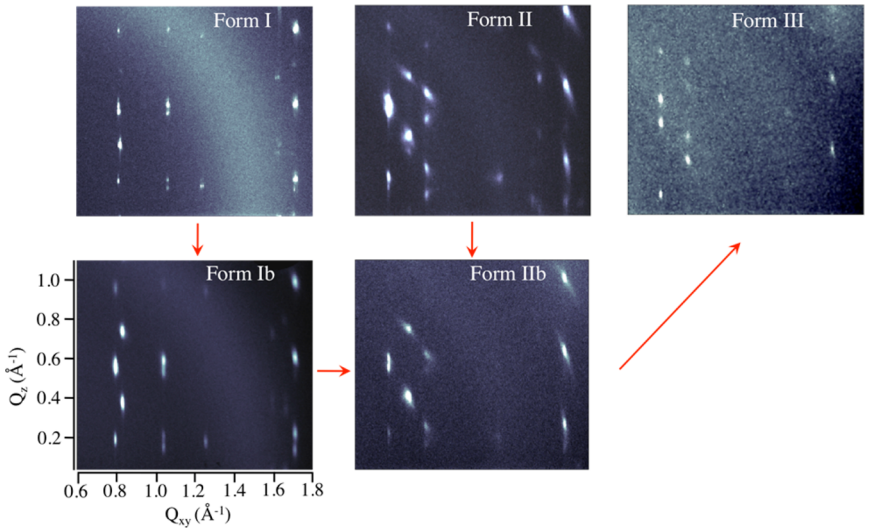

Figure 3. GIXD signatures of the five TIPS-pentacene polymorphs observed. The red arrows indicate the path of transformations activated by thermal energy. Here, Form I was prepared as aligned single-crystalline films using FLUENCE[2] at 50 °C from 8 mg/mL toluene solution, at a shearing speed of 0.25 mm/s. Form Ib was prepared as aligned thin films using solution shearing at 90 °C from 4 mg/mL toluene solution at a shearing speed of 1.6 mm/s. The GIXD images of aligned thin films of I and Ib were taken at room temperature with 360° sample rotation. Form II was prepared as a "2D powder" film using solution shearing at 135 °C from 22 mg/mL mesitylene solution at a shearing speed of 8 mm/s. The diffraction images of Form IIb and Form III were obtained during in situ annealing at 89 and 178 °C, respectively.

spots on the 2D detector representative of all diffraction planes in the sample. Such "2D powder" samples were prepared using the solution shearing method[1,2] in the Landau−Levich regime[22] (see Experimental Methods).

In situ annealing uncovered an unexpectedly rich phase behavior of TIPS-pentacene, revealing the existence of previously unknown polymorphs. Figure 1 shows the solid-to-solid phase transitions activated by thermal energy during annealing (see also SI Movies S1−S3). The samples were equilibrated at each annealing temperature for 10 min. The shifts in the peak positions suggest the changes in the unit cell during polymorphic transitions (Figure 1c), beyond those caused by thermal expansion. From the in situ annealing experiments, three major polymorph transitions, and correspondingly, four polymorphs (I, Ib, IIb and III) can be identified by tracking the peak shift and the variation in the peak width (full width at half-maximum, or fwhm) as a function of temperature (Figure 1d). The method used to assign different classes of polymorphs will be discussed below. The major transition events were distinguished by their differing transition rates, which were correlated with the slope of the Q_{xy}-temperature curve at constant heating rate (Figure 1d). When Ib transformed into IIb, the increase in fwhm is attributed to the coexistence of two polymorphs. During the transition from IIb to III, abrupt changes in both Q_{xy} and fwhm were observed. In particular, Form III peaks became even sharper than before annealing, with fwhm reduced by about half. These observations imply that the IIb-to-III transition occurs via recrystallization (verified by optical microscopy, Figure S1), triggered by the nucleation of the new polymorph within the existing phase. In other words, the transition from IIb to III is a first-order phase transition.

A surprisingly large hysteresis was observed during cooling (Figure 2, SI Movies S4−S6). Form III persisted down to 77 °C before returning to Form IIb, exhibiting a transition temperature hysteresis of approximately 90 °C. Form IIb persisted until the end of the annealing cycle instead of converting back to Form I, indicating a hysteresis larger than 80 °C. Although the existence of hysteresis is expected for first-order polymorph transitions,[23] such large hysteresis is quite unusual. We hypothesize that the nanoscopic confinement effect is a major contributing factor to the large hysteresis observed, which acts via increasing the kinetic barrier to nucleation. To test this hypothesis, we performed in situ annealing experiments (Figure S2) using drop-casted films, which are 300 nm in thickness, as compared to 30 nm solution sheared films. As expected, the hysteresis of both I−IIb and IIb−III transitions were significantly lowered to approximately 25 °C (Figure 2). We also quantified the hysteresis of bulk powders using DSC at a similar scanning rate (10 K/min) as used in the in situ annealing (Figure S3). The hysteresis was further lowered to 3 and 18 °C for the I−IIb and IIb−III transitions, respectively. The nanoconfinement effect is also evident that the transition temperatures decrease with the decrease in characteristic dimensions. This effect is analogous to the melting point depression observed in confined systems.[24] It is due to this confinement effect that we were able to arrest Form II and III at room temperature, despite their highly metastable nature. This allows us to perform a crystal structure determination and charge carrier mobility measurements for these phases. More importantly, such kinetic stabilization makes it possible to use nonequilibrium crystal forms in practical applications.

In addition to the four polymorphs revealed via in situ annealing, we have also observed a fifth polymorph (Form II), which closely resembles Form IIb in its diffraction signature. This polymorph, which we previously reported as a phase exhibiting high hole mobility, was obtained via solution shearing at high T (>127 °C) in films less than 20 nm thick.[2] Again, the confinement effect is key to obtaining Form II in its pure form. Upon heating, Form II transformed to IIb instantaneously (SI Movie S7). The slight shifts of (10), (01), (11) peak positions in Q_z indicate that the main difference between the II and IIb unit cells are in the tilting angle of the c-axis, consistent with the indexing result (Table S1). The major

dx.doi.org/10.1021/ja507179d | J. Am. Chem. Soc. 2014, 136, 17046−17057

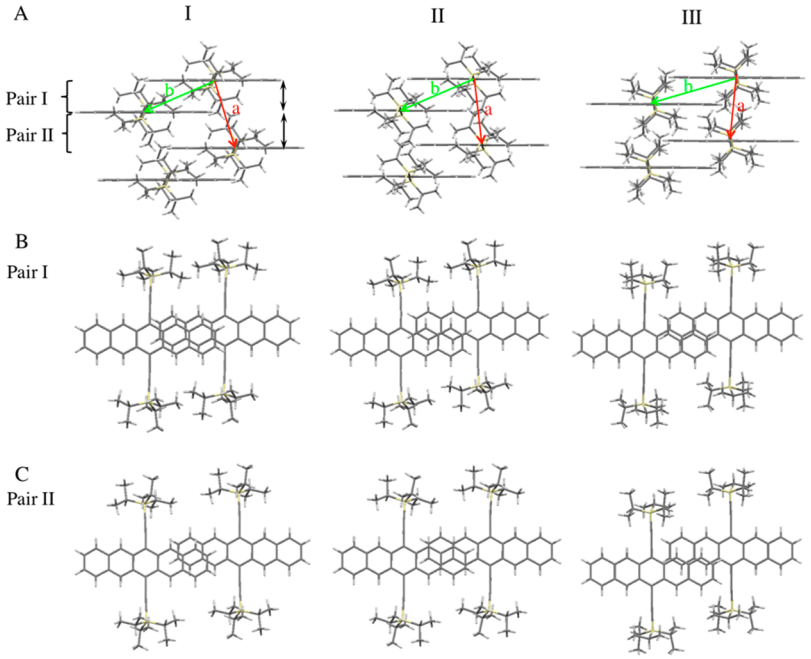

Figure 4. Comparison of the three major polymorphs of TIPS-pentacene in their $\pi-\pi$ stacking (A) and molecular offset along the conjugated backbone (B,C) as obtained from the crystallographic refinement calculations.

distinctions between the two forms are summarized in Figure S7.

In summary, there exist at least five polymorphs of TIPS-pentacene, each exhibiting a distinctive diffraction pattern (Figure 3). Out of the five polymorphs, Form IIb and III have not been reported before. In situ annealing experiments clearly reveal, for the first time, the thermodynamic relationships between the polymorphs (see Discussion). The five polymorphs are categorized into three families: I and Ib, II and IIb, III. Within each family, there is only a slight difference in the unit cells between polymorphs (i.e., a slight change in one or two unit cell parameters), and the polymorph transition is likely to be displacive[25] and probably does not require overcoming a free energy barrier, i.e., is a second order transition. Such transitions are not captured by DSC, indicating that the crystal lattice energies are almost invariant within a family (Figure S3). Between the families, the polymorph transitions are first-order and reconstructive (captured by DSC), resulting in major changes in the unit cell. We next refined the crystal structures to elucidate the difference between the polymorphs at a molecular level.

Crystal Structure Determination. The methodology of thin film structure refinement was detailed in our previous work.[13,26] In this work, a major improvement is made in the refinement methodology by lifting the "rigid molecule" assumption and including the rotational degrees of freedom for the two TIPS side chain moieties (Figure S4). This becomes feasible owing to the large number of diffraction peaks (~30 nondegenerate) observed from samples of high coherence length and high phase purity. Allowing TIPS group rotation improved the structure solution and enabled us to infer the nature of the polymorph transitions.

Sample preparation is very important for obtaining diffraction images with clearly defined, nonoverlapping peaks. This enables us to resolve subtle differences in the unit cell geometries can be resolved as well as to obtain statistically reliable peak intensities for structure refinement. Samples with large crystalline domains of high coherence length and high phase purity are desired to yield a large number of sharp diffraction peaks. The "2D powder" samples used in in situ annealing experiments often fall short of these requirements as do the evaporated samples, in both cases due to peak broadening as a result of small domain sizes and low coherence lengths. To prepare high quality films, the FLUENCE technique[2] was used to produce aligned, single-crystalline films. In order to remove the influence of in-plane texture in the highly aligned films, the samples were made circular and rotated in-plane during the data collection. The thus collected data were compared against those obtained from "2D powder" samples and evaporated samples to make sure the relative peak intensities were comparable. The conditions used for isolating each pure polymorph are summarized in the Experimental Methods.

The unit cell indexing results are summarized in Table S1. Comparing three major polymorphs (I, II, III), the main differences are in the length of b-axis and the α, γ angles. Within each family of polymorphs, the changes in the unit cell are slight. With the unit cell and peak intensity information, we next carried out structure refinement to determine the angular alignments of the pentacene core and the TIPS side group in the unit cell by minimizing the crystallographic residual (a type of least-squares error between the theoretical and experimental intensity values). In this work, we focus on solving the structures of Form II and III. Form I and Ib refinement results were published in our previous work,[1,26] whose structures closely resemble that of the bulk single crystal.[21] Form IIb was only observed during in situ annealing. The quality of diffraction data was insufficient for carrying out structure refinement, as mentioned above. For both Form II and III, the calculated diffraction intensities (of the best-fit structure) match well with the measured intensities within experimental error (Figure S5). Allowing the TIPS group rotation markedly improves the refinement result (Figure S6). The crystallographic residual lowered by 12% in the case of Form II, and by

dx.doi.org/10.1021/ja507179d | J. Am. Chem. Soc. 2014, 136, 17046−17057

almost 50% for Form III as the TIPS group "clicked" into a new angular position of approximately 127° with respect to that of the bulk crystal structure (SI Movie S8). Molecular mechanics calculations corroborate this observation, namely that the new angular position of the TIPS group lowers the lattice energy by 0.37 eV. These results indicate that TIPS-pentacene is likely to assume a substantially different molecular conformation in Form III. We speculate that side chain conformation change is an important driving force for polymorph transitions of TIPS-pentacene (see Discussion).

The differences in the molecular packing of the three major polymorphs are summarized in Figure 4. Both the $\pi-\pi$ stacking distance and intermolecular offset significantly vary among the three polymorphs. Compared to Form I, the $\pi-\pi$ stacking distances are reduced for both molecular pairs of Form II (Table 1). Interestingly, Form III exhibits a record low $\pi-\pi$ stacking distance (pair I) of less than 3 Å; however, this comes at the expense of a greatly reduced orbital overlap in both pairs. These changes in crystal structures are expected to bring profound changes in the thermodynamic and electronic properties. We next investigate the energy landscapes of TIPS-pentacene using molecular mechanics simulations and quantify the differences in electronic properties via charge transfer integral calculations and charge carrier mobility measurements.

Table 1. Comparison of $\pi-\pi$ Stacking Distances of Forms I–III

$\pi-\pi$ stacking (Å)	pair I	pair II
Form I[a]	3.30	3.89
Form II	3.23 ± 0.06	3.65 ± 0.07
Form III	2.82 ± 0.13	3.75 ± 0.14

[a]Ref 1. Form I was obtained by solvent vapor relaxing from Form II. Error bars are estimated from sample to sample variations in measured peak intensities and from structure refinement.

Computational Predictions of Polymorph Forms. Predicting the structure of polymorph forms of organic molecules a priori using computation is not a straightforward task if, as here, no experimental information from the experimental studies described above is used to help guide the results. The approach essentially involves providing a suitable inter- and intramolecular model for the TIPS-pentacene molecule and using this to predict the energy of the system as the geometry of the unit cell is varied to reveal the lowest energy structures.

Accordingly, we modeled TIPS-pentacene via Avogadro and TINKER[27,28] using the Allinger et al. MM3 semiempirical potential[29] that we have found works well for representing the intermolecular forces in "small molecule" organic semiconductors. Using an ab initio representation of the molecules to systematically vary all parameters of a unit cell of TIPS-pentacene molecules would have been a prohibitively expensive undertaking. The parametrization of the MM3 potential for TIPS-pentacene is described in the Supporting Information (Figures S8 and S9, Tables S2 and S3). Validation of the MM3 model against our ab initio calculations is also provided in the SI.

For our "energy baseline" reference study, we constructed a computational description of a unit cell of four TIPS-pentacene molecules using values for $[a, b, \gamma]$ that represent the bulk single crystal for the equilibrium as reported by Anthony et al.:[21] a-axis = 7.75 Å; b-axis = 7.56 Å; and γ = 96.4° (note: this set of unit cell parameters is equivalent to a = 7.56 Å, b = 7.75 Å, γ = 83.6°). The c-axis was set to 1000 Å in order to simulate a two-dimensional structure. The energy of this unit cell was then minimized in TINKER and was used as the reference point for the energy difference quoted in all subsequent calculations. As a further test of the models, we used a completely independent Bayesian optimization method, conducted by a collaborator.[30] This study was able to locate the lowest energy of the system and confirm that the corresponding $[a, b, \gamma]$ parameters were close to the experimental results for polymorph I.

To determine the location of any other polymorphs we scanned the energy landscape as we varied the $[a, b, \gamma]$ parameters. We explored the effect of varying these three parameters in the following broad ranges: 7.2–8.1 Å for the a-axis; 7.2–9.36 Å for the b-axis; and 72–116° for γ, without assuming any prior knowledge of the locations of the polymorphs. Each choice of $[a, b, \gamma]$ was submitted to an energy minimization calculation within TINKER, and then the reference equilibrium energy was subtracted from the resulting configurational energy relevant to that $[a, b, \gamma]$ choice. This produced an energy landscape that was composed of many (more than five) narrow fractal-like energy minima that were close in energy. While such landscapes may seem to be atypical for crystal structure searches in general, our findings are reminiscent of the energy landscape of fractal glasses,[31] which describes the existence of energy "metabasins."

Given the rich, rather fractal-looking, energy landscape which we observed computationally, one that includes many more "metabasins" than the five reported experimentally, we mapped

Table 2. Comparison of Experimental and Calculated Parameters for the Five Lowest Energy States and Polymorph Identification

polymorph	a (Å)	b (Å)	γ (deg)	ΔE (eV)	ΔE_{offset} (eV)
I (expt)	7.68	7.77	81.46	–	–
I (calc) (expt − calc)	7.56 (0.1)	8.00 (−0.2)	80.0 (1.5)	−1.22	0
Ib (expt)	7.67	7.91	80.25	–	–
Ib (calc) (expt − calc)	7.56 (0.1)	8.10 (−0.2)	80.0 (0.2)	−1.20	0.02
II (expt)	7.48	8.50	71.29	–	–
II (calc) (expt − calc)	7.75 (−0.3)	8.40 (0.1)	68.0 (3.3)	−1.16	0.06
IIb (expt)	7.57	8.59	71.67	–	–
IIb (calc) (expt − calc)	7.76 (−0.2)	8.64 (−0.05)	68.0 (3.7)	−1.15	0.07
III (expt.)	7.56	9.02	65.23	–	–
III (calc) (expt − calc)	7.75 (−0.2)	8.64 (0.4)	63.9 (1.3)	−1.13	0.09

dx.doi.org/10.1021/ja507179d | J. Am. Chem. Soc. 2014, 136, 17046–17057

our *five lowest energy* polymorphs (without any picking and choosing among energy minima) to the five polymorphs that the experimentalists found and observed that they were close in terms of [*a*, *b*, *γ*] values. These results are shown in Table 2. ΔE_{offset} is the difference in ΔE for the polymorphs using the ΔE of polymorph I as the baseline. We estimate the uncertainty in the energies to be between 0.01 and 0.02 eV. Thus, we can, with some confidence, distinguish between the three major families of polymorphs (I, II, III), but distinguishing the polymorphs within each family is not possible since the differences in relative energies lie within our estimated uncertainty.

As can be seen in Table 2, the computed unit cell parameters of these five lowest energy structures compare well against the experimental data: differences in "*a*" and "*b*" are around 0.1−0.2 Å (2−3%) and those in *γ* are, at worst, <4° (<5%). The computationally predicted relative energies of the three major polymorphs match qualitatively with the DSC data (Figure S3). Given that finding the crystal structure for a molecule like TIPS-pentacene is particularly challenging due to the conformational flexibility of the molecule (FiguresS16−S21), the degree of agreement with the experimental data is very encouraging. It is important to note here that this quality of agreement with experiment is far from guaranteed. Indeed, the appropriateness of the force field to accurately represent the material plays a critical role here, as might be expected from such energetically similar polymorphs. For example, our attempts to model TIPS-pentacene with the OPLS force field did not show the same high caliber of correspondence with experiment.

Furthermore, we investigated whether the energy minimum is isotropic across all three parameters; that is, is the minimum "bowl" shaped or does it resemble a valley floor? This provides information regarding which of the [*a*, *b*, *γ*] parameters is "sloppy"[32,33] (poorly constrained) and which are "stiff" (highly constrained) directions. It can be seen that, in general, the energy landscape is not isotropic (Figure S10). Overall, the topology of the energy landscape is such that it is less sensitive to changes in *a* and *b* than changes in *γ*. To repeat the metaphor used above, the energy profile is not an isotropic bowl shape but a valley floor in which changes in *a* and *b* are "sloppy,"[34] but changes in *γ* are stiff. This computational finding is consistent with the in situ annealing (Figure 2) and the unit cell indexing results (Table S1) that *γ* is the main unit cell parameter distinguishing three families of polymorphs.

Finally, we predicted the *π*−*π* stacking distances of Forms I−III for the two pairs of TIPS-pentacene molecules as a final point of comparison with experiment. The results of these predicted distances are shown in Table S4. In general, the difference between the experimental distances and the computationally predicted values for pair-II were quite good (around 0.4 Å). They were also very good for pair-I for polymorph Form I (a difference of 0.1 Å), but increasingly poor for polymorph Forms II and III (differences of 0.9 and 1.4 Å). Overall, the differences are satisfactory.

Charge Transport Properties. The ability of TIPS-pentacene to assume multiple crystal structures offers an opportunity to study the impact of molecular packing on charge transport properties without changing the molecular structure. Table 3 summarizes the charge transfer integrals of three major polymorphs calculated using density functional theory (DFT) (see Experimental Methods). The differences in electronic couplings among the polymorphs are substantial, attesting to the sensitivity of charge transport to molecular packing. The difference in the electronic coupling also manifested in the UV−vis absorption spectra (Figure S11) at high wavelengths (500−750 nm), which corresponds to excitations to the first singlet excited state (S_0−S_1).[35] The calculated charge transfer integrals are qualitatively consistent with the charge carrier mobilities measured in our work and reported in the literature (Table 4). Interestingly, DFT calculations predict that TIPS-pentacene may switch from a well-established p-type semiconductor to n-type when crystallized in Form III, given the high electron transfer integral of pair II (Table 3).

Table 3. Comparison of Charge Transfer Integrals for Unique Molecular Pairs in the Crystal Structures of Three Major Polymorphs

polymorph	molecular pair[a]	center-of-mass distance (Å)	hole transfer integral (meV)	electron transfer integral (meV)
Form I	Pair I	7.8	10.6	−131.7
	Pair II	10.2	17.9	−41.1
Form II	Pair I	8.5	34.3	30.6
	Pair II	9.3	−54.1	62.7
Form III	Pair I	9.0	1.3	0.4
	Pair II	9.0	18.9	−174.7

[a]Pair I and II are unique molecular pairs identified in Figure 4.

Table 4. Comparison of Charge Carrier Mobilities of Three Major Polymorphs[a]

	hole mobility ($cm^2\ V^{-1}\ s^{-1}$)		electron mobility ($cm^2\ V^{-1}\ s^{-1}$)	
polymorph	average	max	average	max
Form I	2.4 ± 0.6[37]	3.8	3.2 ± 1.47[38]	6.81
Form II	8.1 ± 1.2[2]	11		
Form III	(5.8 ± 0.4) × 10^{-2}	0.09		

[a]All data listed were obtained using a top-contact, bottom-gate device configuration. The hole motilities of Form I and II listed are the highest reported in the literature, using solution processed single crystal devices. The electron mobility of Form I was determined from a doped polycrystalline device. Form III hole mobility was evaluated in this work, using 2−4 monolayer thick thin films.

The evaluation of Form III devices has posed a major challenge, largely due to the highly metastable nature of this polymorph at ambient conditions. Although Form III is attainable when the film is subjected to thermal treatment, it inevitably converts back to Form II or I even when quench cooled in liquid nitrogen. This observation attests to the high metastability of Form III at low temperature. Ultimately, we managed to arrest Form III in thin films at room temperature by a combination of confinement effect[36] and kinetic trapping.[19] As found in the in situ annealing study, the nanoconfinement effect enhanced the kinetic stability of Form III. This effect became a key enabler for obtaining Form III at low temperature. As a result of this strategy, only when the films are as thin as 1−3 monolayers can Form III be stabilized in its pure form (Figure 5a). We then significantly improved the film morphology of Form III thin films using FLUENCE, a technique we developed recently[2] (Figure 5b). The hole transport characteristics of Form III ultrathin films are summarized in Figure S13.

In addition to TIPS-pentacene, we demonstrated our methodology using a [1]benzothieno[3,2-*b*][1]1benzothiophene (BTBT) derivative, whose molecular packing adopts a herringbone motif, substantially different from the brick-wall

dx.doi.org/10.1021/ja507179d | J. Am. Chem. Soc. 2014, 136, 17046−17057

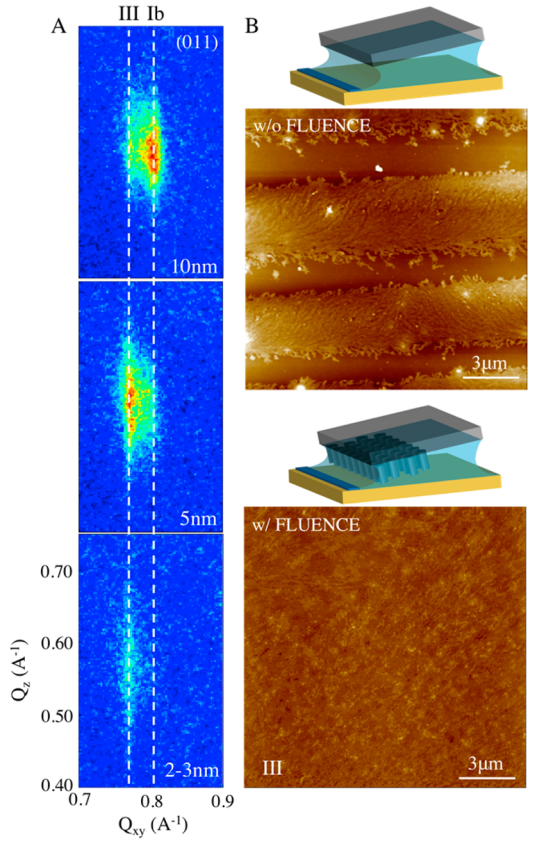

Figure 5. Arresting Form III thin films at room temperature for charge carrier mobility measurements, using confinement effect (A) combined with the FLUENCE technique (B). A) GIXD images of solution sheared TIPS-pentacene thin films under nanoconfinement. The (011) reflection is shown in all images. The two white dotted lines indicate the Q_{xy} positions of (011) peak corresponding to Form III and Ib. The molecular packing of TIPS-pentacene evolved from a mixture of Form Ib, II, III to pure Form III, when the film thickness decreased from 10 nm to 2–3 nm. Full GIXD image of Form III is shown in Figure S12. The films were solution sheared on PTS treated Si wafer from 50 °C TIPS-pentacene/toluene solution at 2 mm/s, at solution concentrations of 16, 8, 4 mg/mL (top to bottom). (B) AFM height images of Form III thin films prepared without (top) and with (bottom) FLUENCE. The film morphology is much improved when prepared with FLUENCE. The films were prepared using solution shearing of 0.2 mg/mL TIPS-pentacene/chloroform solution at 60 °C, at shearing speed of 1 mm/s. This condition falls under the evaporation regime, which is conducive to domain alignment favorable to charge transport.

packing of TIPS-pentacene. In situ annealing uncovered two polymorphs of this compound (Figure S14), Form II being metastable at ambient conditions. Using the nanoconfinement effect, we were able to stabilize Form II at room temperature (Figure S15), attesting to the generality of our approach.

DISCUSSION

The in situ annealing results combined with molecular simulation and the DSC data inform the thermodynamic underpinnings of TIPS-pentacene polymorphism. The molecular origin of the polymorph transitions can be further inferred from the molecular simulation and structural refinement results. In addition, we discuss in brief the implications of our findings on improving the charge transport properties of organic semiconductors.

First, we discuss the thermodynamic relationships between the five TIPS-pentacene polymorphs (Figure 6). In terms of the

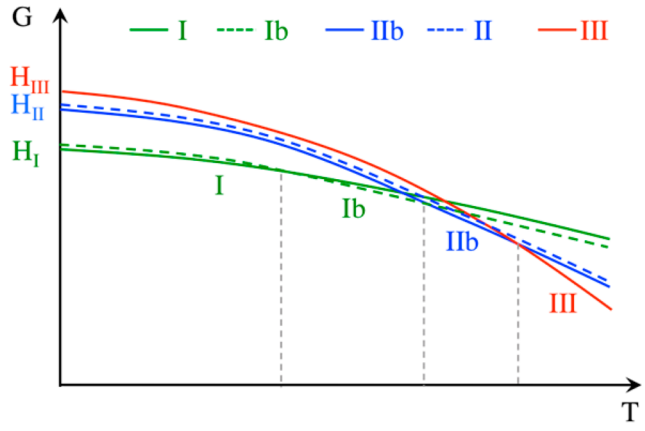

Figure 6. Qualitative thermodynamic energy–temperature diagram for the transition among TIPS-pentacene polymorphs. The intercept of the curves with the *y*-axis is the enthalpy (H), and the slope of the curve is the entropy. The transition temperatures are not labeled because they are dependent upon the film thickness, a.k.a., are functions of the confinement effect (Figure 2).

thermodynamic properties, polymorphism can be categorized into enantiotropic and monotropic systems. Enantiotropic systems exhibit crystal forms whose stability switch reversibly across a transition temperature below the melting point. On the other hand, a monotropic system possesses only one stable crystal form and the transition between polymorphs is irreversible. Inferred from the in situ annealing data, Form I, Ib, IIb and III follow the enantiotropic relationship, whereas Form IIb and II are monotropically linked, since Form II is metastable across the accessible temperature range and cannot be accessed via thermal annealing (Figure 6). The enthalpic relationship between the polymorphs can be estimated from the molecular mechanical calculations (Table 2) and measured by DSC (Figure S3). The difference in lattice energy is 37.3 meV between Form I and II, and merely 5.7 meV between Form II and III as measured by DSC, which is qualitatively consistent with the calculated results. These sources of information together paint a qualitative free energy-temperature diagram shown in Figure 6. It is worth noting that the energetic differences between the polymorphs are very small, only on the order of k_BT. However, the impact on electronic performances is at the same time significant, highlighting the importance and the challenge of controlling polymorphism. Free energy diagrams (e.g., Figure 6) will certainly facilitate rational design approaches for controlling polymorphism.

Next, we discuss the type of the polymorphic transitions observed. Polymorphic transformations can be categorized by the order of the phase transition (first or second order), or by the types of structural changes involved. We infer that within each polymorph family, the structural transitions (I–Ib, II–IIb) are second-order and displacive in nature, whereas between the families (I–IIb, IIb–III), the transformations are first-order and reconstructive. This is evidenced by the fact that the transformations within the family are gradual (in situ annealing), do not involve detectable changes in the lattice energy (no DSC signature; Figure S3), do not exhibit apparent barriers to transformation (no hysteresis during annealing) and result in only slight changes in the unit cell (Table S1). In

dx.doi.org/10.1021/ja507179d | J. Am. Chem. Soc. 2014, 136, 17046–17057

contrast, the transformations between the families are abrupt, involve observable change in lattice energies, exhibit free energy barriers to transformation (hysteresis observed during annealing) and produce substantial change in the unit cell.

What is the molecular origin of the rich polymorphic behavior of TIPS-pentacene? We speculate that the structural diversity of TIPS-pentacene is closely related to the conformational flexibility of the side chains. In the case of pentacene, only two polymorphs were observed during an annealing study.[39] In TIPS-pentacene, our structure refinement results indicate that the TIPS group adopts a substantially different conformation in Form III, the new polymorph observed in this study. The conformational change of the side chains could be a main driving force for the polymorphic transformation between IIb and III. This hypothesis is further explored using molecular mechanics simulations as discussed below.

First of all, molecular mechanics simulations reveal that it is possible to predict all five of the Forms (I, Ib, II, IIb, and III) as the five lowest energy structures (Table 2), within a rich fractal-like set of narrow metabasins in a broader energy landscape than can be explored experimentally. The computational predictions were made in an unbiased, experimentally uninformed manner that gives them credence and rigor. The corresponding unit cell parameters predicted for these five structures closely resemble the experimental results. The energetic separation of the computationally predicted polymorphs also mirrors the experimental findings. Comparison of the computationally predicted $\pi-\pi$ stacking distances of Forms I–III also show a pretty good representation of the experimental values. In addition, the stiff direction identified by the molecular mechanics, γ, is also identified as such in the experiments. Given the conformational flexibility of TIPS-pentacene and the fact that the semiempirical intermolecular potential models will not be a perfect representation of the real molecule, this excellent correspondence is by no means a foregone conclusion. Indeed, the quality of the reproduction of the polymorphs by the computational predictions is remarkable and could not have been expected.

The close match of the molecular mechanics simulations with the experimental data allowed us to further investigate the molecular origin driving their formation. We found that there was a correlation between minimizing the strain in the molecule and the location in $[a, b, \gamma]$ space of the major polymorphs. That is, as we changed $[a, b, \gamma]$ values, we observed the acene backbone to bend and twist by a couple of degrees, as well as changes in the rotation of the methyl groups and the silyl-ethynyl angle in the TIPS functional group (Figure S16–S21). It is not clear which of these three structural changes (backbone distortion, methyl group rotation or TIPS group wagging) is primarily responsible. However, several observations helped us create a reasonable picture of the sequence of events that led to the energetic preference of a particular polymorph: First, the largest strain is encountered when the TIPS group wags or rotates. Second, the degree of twisting observed here in the acene backbone was not observed in our earlier computational studies of the parent pentacene molecules. This suggests that the acene backbone changes are an effect rather than a cause. Given the bulkiness of the TIPS group, and the resulting steric hindrance, this conclusion seems intuitively reasonable. Piecing these information together, we speculate that we are seeing a "domino effect": the methyl groups that constitute the TIPS group rotate, but the hindrance due to the close contact with another TIPS-group causes the silyl-ethynyl groups to wag and the entire TIPS-group to rotate. As the TIPS group establishes a new conformation, they induce strain into the acene backbone causing it to bend and twist slightly. This, we propose, affects the energy landscape. Evidence for this connection between minimizing strain in the TIPS-pentacene molecule and the energy landscape is provided when considering that the minima for the angular differences (i.e., a minimization of the strain) aligned closely with the minima of the energy profiles.

■ CONCLUSIONS

In summary, we elucidate organic semiconductor polymorphism combining advanced synchrotron X-ray techniques with molecular simulations and quantum chemical calculations with charge carrier mobility measurements. This is made possible by enhancing the kinetic stability of highly metastable polymorphs via the nanoconfinement effect. Using this method, we were able to stabilize a highly metastable polymorph of TIPS-pentacene for structural and charge transport studies. In addition, we also demonstrated this methodology using a [1]benzothieno[3,2-*b*][1]1benzothiophene (BTBT) derivative.

We carried out in-depth investigations to unravel the polymorphism of TIPS-pentacene. Specifically, we were able to identify a new polymorph (Form III) for TIPS-pentacene, an extensively studied organic semiconductor. Crystal structure obtained from thin film refinement revealed a different side chain conformation and an extremely close $\pi-\pi$ stacking distance in the new polymorph of less than 3 Å. In total, three distinctive families of polymorphs of TIPS-pentacene are unraveled (I, II, III), via both in situ X-ray diffraction and molecular simulations. The relative energy and unit cell parameters of polymorphs predicted independently by molecular simulations closely matched the experimental observations. Additionally, based on structural refinement and molecular simulations, we propose that the molecular origin of the polymorphism of TIPS-pentacene is the conformational flexibility of the side chains.

The structural diversity of TIPS-pentacene offers an intriguing example for studying structure–property relationships in organic semiconductor systems. Even with the same packing motif, small changes in molecular packing showed a profound impact on the electronic coupling and therefore the charge transport properties of the system. The calculated charge transfer integral varies substantially across different polymorphs, which explains several orders of magnitude difference in the measured hole mobility. This example also shows that the equilibrium molecular packing at room temperature is not necessarily the one with the best charge transport properties. In the case of TIPS-pentacene, the highest hole mobility was obtained in Form II, a metastable form at ambient conditions. Thanks to the confinement effect, the drastically enhanced kinetic stability of nonequilibrium forms opens avenues for their applications in actual electronic devices, in addition to granting access to transient metastable forms for fundamental studies of crystal polymorphism and structure–property relationships.

■ EXPERIMENTAL METHODS

In Situ Annealing. "2D powder" samples were prepared for in situ annealing experiments using the solution shearing method[1,2] in the Landau–Levich regime.[22] In the Landau–Levich regime, spherulite crystallization occurs because the solution shearing speed is so fast that it outruns the solvent evaporation. Therefore, a liquid film forms first

dx.doi.org/10.1021/ja507179d | J. Am. Chem. Soc. 2014, 136, 17046–17057

Table 5. Conditions for Isolating TIPS-Pentacene Polymorphs

form	aligned thin film	"2D powder" thin film
I	FLUENCE[2] coated at 0.2 mm/s from 50 °C, 8 mg/mL toluene solution (used for indexing).	Sheared at 2.5 mm/s from 50 °C, 30 mg/mL toluene solution.
Ib[a]	FLUENCE[2] coated at 1.6 mm/s from 90 °C, 2 mg/mL toluene solution (used for indexing).	Thermally converted from Form I at 89 °C.
II	FLUENCE[2] coated at 0.8 mm/s from 135 °C, 1.6 mg/mL mesitylene solution. Alternatively, sheared at 1.6 mm/s from 135 °C, 8 mg/mL mesitylene solution (used for indexing and refinement).	Sheared at 8 mm/s from 135 °C, 22 mg/mL mesitylene solution.
IIb	Thermally converted from Form II at 89 °C. This form has not been directly obtained using solution shearing (used for indexing).	
III	FLUENCE[2] coated at 1 mm/s from 60 °C, 0.2 mg/mL chloroform solution. The gap size is set to be 100 μm, and the blade tilting angle is 8°. The resulting film thickness is 3.2−4.8 nm, which is too thin for refinement purpose. Instead, these films are used for charge transport measurements.	(1) Anneal PVP40 capped thin film of Form I 2D powder sample to above 190 °C to induce recrystallization of Form III, then cool to ∼100 °C. The resulting film comprises of numerous discrete crystallites of a few microns in diameter, misoriented in-plane, but highly oriented out-of-plane. The corresponding GIXD patterns are used for refinement. (2) Sheared at 2 mm/s from 50C, 4 mg/mL toluene solution. The gap size is set to be 100 μm, and the blade tilting angle is 8°. The resulting film thickness is 2.5 ± 0.4 nm. The corresponding GIXD patterns of films at room temperature are used to verify peak positions and intensities of samples prepared using method (1).

[a]Also obtained via thermal evaporation.[26]

and subsequently nucleation occurs sporadically throughout the film, followed by spherulitic growth. Form I "2D powder" thin film samples were prepared via solution shearing at a substrate temperature of 50 °C, with a shearing speed of 2.5 mm/s, using the 30 mg/mL TIPS-pentacene (Sigma-Aldrich) solution dissolved in toluene (ACS grade). The front of the shearing blade was separated from the substrate by 100 μm (gap size), with a blade tilting angle of 8°. The resulting film was 34.4 ± 3.6 nm in thickness. Once the film was prepared, a capping layer was spin-coated on top of the solution-sheared TIPS-pentacene film. For spin-coating, 15 wt % aqueous solution of PVP40 (polyvinylpyrrolidone with an average molecular weight of 40 000; Sigma-Aldrich) was prepared by stirring the PVP40/DI water mixture overnight followed by filtration using the 0.45 μm PVDF syringe filter. A drop of 100−200 μL PVP40 solution was spread over the film and spin-coated at a speed of 4000 rpm. The capped film was then baked at 100 °C for 30 min to remove residue water left in the capping layer, and then slowly cooled down to room temperature. This annealing procedure did not change the molecular packing of the film as verified by grazing incidence X-ray diffraction (GIXD). The resulting capping layer thickness was 268 ± 10 nm. Various materials were used for the capping layer to verify that the chemical makeup of the capping layer does not interfere with the in situ annealing result of the semiconductor layer. These materials include: CYTOP (spin-coated), poly(vinyl alcohol) of various molecular weight cross-linked by ammonium dichromate (spin-coated), polyvinylpyrrolidone of various molecular weight (spin-coated), lithium floride (thermal evaporated). Form II "2D powder" thin film samples were prepared following a similar procedure. The solution shearing was performed using 22 mg/mL mesitylene solution, at a substrate temperature of 135 °C, and a shearing speed of 8 mm/s.

Form I "2D powder" thin films were prepared at various thickness to investigate the dependence of polymorph transition temperature hysteresis on film thickness. Thinnest films were prepared by solution shearing of 30 mg/mL toluene solution at a substrate temperature of 50 °C, at a shearing speed of 2.5 mm/s. The resulting film thickness was 34.4 ± 3.6 nm. The film of intermediate thickness was solution-sheared at a substrate temperature of 50 °C, at a shearing speed of 3 mm/s, using the 100 mg/mL toluene solution. The resulting film was 112 ± 29 nm in thickness. In both cases, the front of the shearing blade was separated from the substrate by 100 μm (gap size), with a blade tilting angle of 8°. The thickest film was dropcast from 100 mg/mL toluene solution at room temperature, the resulting film thickness was around 300 nm.

For in situ annealing of the aforementioned samples, grazing incidence X-ray diffraction (GIXD) measurements were performed at the Stanford Synchrotron Radiation Lightsource (SSRL) at beamline 11−3. An area detector (MAR345 image plate) was placed approximately 400 mm away from the center of the sample. The beam energy was 12.73 keV. The incident angle was set as 0.12°. The scans were performed on a heated stage under helium protection. At each temperature set point, the sample was equilibrated for 10 min and no peak shift was observed beyond this point. The temperature was increased from room temperature to 204 °C and then decreased back to room temperature at approximately 10 °C intervals to complete an annealing cycle. The thus obtained 2D diffraction patterns were analyzed using the wxDiff software.

Structure Refinement. Thin film samples with millimeter sized, aligned single-crystalline domains were prepared for crystal unit cell indexing and crystal structure refinement (except for Form III) using FLUENCE. The film preparation procedures for isolating each pure polymorphic phase are summarized in Table 5.

The as prepared samples were cut into small pieces of approximately 3 × 3 mm^2 in size to reduce the peak broadening from the long beam path. The active sample area was made circular by placing a circular shadow mask over the film and removing the active layer when exposed to O_2 plasma at 150 W, 150 mTorr for 1.5 min. The circular shape is important for obtaining statistically averaged peak intensities during X-ray exposure with sample rotation. GIXD scans were performed at beamline 1−5 of SSRL at SLAC, equipped with a 360-degree rotational sample stage. The beam energy was set as 12.7 keV, and the sample to detector (MAR345 image plate) distance was approximately 400 mm. The incident angle of the X-ray was set to be 0.12°. At least three samples were scanned for each solution shearing condition.

The detailed procedure of the crystal structure refinement can be found in our previous work.[26] In this work, we added the ability to our refinement software to rotate moieties on the molecule about specified bonds in order to capture some of the molecule's conformational flexibility. Specific bonds can be designated to act as a "hinge" allowing the rotation of the atom clouds on either side of the hinge. In the specific case of TIPS-pentacene, the rotation of triisopropyl "crown" was added as an additional degree of freedom to the calculations while centrosymmetry however was still enforced. The Monte Carlo optimization of the crystallographic residual was performed with an in-house developed software, POWERGRID.[40]

The reliability of the refinement results was verified as the following. GIXD patterns of more than 10 different samples were compared to verify the relative peak intensities and peak positions. Furthermore, for refinement of each polymorph, GIXD patterns obtained from rotational scans of single-crystalline samples at beamline 1−5 are compared against corresponding diffraction patterns from static 2D powder samples obtained at beamline 11−3. In addition, consistency was also checked by comparing GIXD patterns of the same polymorph obtained via thermal transformation, with those of solution sheared samples. These consistency checks helped to eliminate potential errors from preferred orientation of "2D powder" samples, and from noncircular shape of aligned single-crystalline samples. Both of the two errors could skew the relative peak intensities and therefore the

refinement results. In this work, these two sources of errors were found to be insignificant in our samples used for refinement.

Charge Transfer Integral Calculations. Density functional theory (DFT) calculations were performed using the Becke, 3-parameter, Lee–Yang–Parr functional (B3LYP)[41,42] with a 6-31G** basis.[43] Charge transfer integrals were calculated using the projective method.[44] A total of 8 unique transport pathways were calculated for each Form, but only the π-stacking pairs displayed in Table 3 showed transfer integrals >3 meV. All DFT calculations were performed employing the ORCA v2.9.1 software package.[45]

Transistor Device Characterizations. For hole mobility assessment of the newly observed polymorph Form III, the films were prepared via solution shearing of 0.2 mg/mL TIPS-pentacene/chloroform solution at shearing speed of 1 mm/s. FLUENCE technique was applied to yield continuous films of only 4 nm nominal thickness. We found that the thinness of the film and rapid shearing speed are critical for isolating the pure form of polymorph III at room temperature. Either reducing the shearing speed or increasing the shearing temperature led to mixture of multiple polymorphs, typically Form I, Ib and/or III. These observations indicate that confinement effect combined with kinetic trapping is critical for obtaining highly metastable polymorphs.

Devices were fabricated in the top-contact, bottom-gate configuration, with Au drain and source electrodes (40 nm) and PTS-modified SiO_2 dielectric layers (300 nm). Two channel lengths were tested, 50 and 5 μm. The 50 μm channel length devices were fabricated using the shadow masks with channel widths of 1000 μm, whereas the 5 μm channel length devices were made using perylene masks with channel width of 200 μm. The electrical characterization was performed using a Keithley 4200-SCS semiconductor parameter analyzer. Devices were fabricated in ambient conditions and tested in N_2 filled glovebox.

The electron mobility measurements were performed using solution sheared TIPS-pentacene film doped with 2-(2-methoxyphenyl)-1,3-dimethyl-2,3-dihydro-1*H*-benzoimidazole (o-MeO-DMBI). The detailed procedure was reported in our previous work.[38] Briefly, 8 mg/mL doped TIPS-pentacene solution was prepared using dry toluene under N_2 protection. Subsequently solution shearing was performed at 60 °C at 0.4 mm/s on divinyltetramethyldisiloxane bis(benzocyclobutene) (BCB) coated SiO_2 substrates. The resulting TIPS-pentacene films were identified as Form I via GIXD. After electrodes were deposited, the samples were annealed at 90 °C under a nitrogen atmosphere for 1.5 h to thermally dissociate the dopant into its active form for electrical characterizations. Without dopants, n-type transistor characteristics were not observed in TIPS-pentacene films. We attempted to measure electron mobility in films of Forms II and III. In the case of Form II, the films need to be prepared at 135 °C from mesitylene solution. At this high temperature, the dopants were already dissociated during solution shearing in atmosphere, and were rendered ineffective before devices can be fabricated and tested, due to the presence of oxygen. For Form III, the films were highly unstable at elevated temperature and therefore could not withstand the annealing step at 90 °C.

Sample Characterizations. DSC measurements were performed on a Mettler-Toledo DSC1 STARe differential scanning calorimeter under dry nitrogen atmosphere, using as purchased TIPS-pentacene bulk powders. Temperature calibration was performed before experiments using indium as a standard. Optical characterization of the films was done using an Agilent Cary 6000i UV/vis/NIR spectrometer equipped with an InGaAs detector. Spectra were obtained within a wavelength range of 800 to 250 nm. Tapping-mode AFM images of the films were recorded using a Multimode Nanoscope III with Extender electronics (Digital Instruments/Veeco Metrology Group, Santa Barbara, CA).

For details of the molecular mechanic simulations, see Supporting Information (section "MM3 parametrization"; Figure S8, S9, and Tables S2, S3).

■ ASSOCIATED CONTENT

Ⓢ Supporting Information

Details of the crystal structure refinement, DSC data, details of the molecular mechanic calcuations, UV–vis data, transistor device characterizations, annealing results of the BTBT derivative, and computational study on molecular conformation change. This material is available free of charge via the Internet at http://pubs.acs.org.

■ AUTHOR INFORMATION

Corresponding Authors

stefan.mannsfeld@tu-dresden.de
zbao@stanford.edu

Notes

The authors declare no competing financial interest.

■ ACKNOWLEDGMENTS

Y.D. acknowledges the initial support from a seed grant by the Department of Energy, Laboratory Directed Research and Development funding, under Contract DE-AC02-76SF00515 and subsequent support by the Department of Energy, Bridging Research Interactions through collaborative Development Grants in Energy (BRIDGE) program under Contract DE-FOA-0000654-1588. We are grateful to Dr. Michael Toney at Stanford Synchrotron Radiation Lightsource (SSRL) for valuable input. We give thanks to J. E. Anthony and M. M. Nelson of 3M Corp. for providing high-purity TIPS-pentacene. We appreciate helpful discussions with Prof. John Anthony from Department of Chemistry at University of Kentucky. Portions of this research were carried out at the Stanford Synchrotron Radiation Lightsource, a national user facility operated by Stanford University on behalf of the US DOE, Office of Basic Energy Sciences. S.P. and Z.B. acknowledge support by the National Science Foundation (DMR-1303178). K.M.L. and P.C. acknowledge support by an Intel Foundation/SRCEA Masters Scholarship. W.-Y.L. acknowledges postdoctoral fellowship support from Postdoctoral Research Abroad Program sponsored by the National Science Council, Taiwan. M.B.-F. acknowledges support by the US Department of Energy Office of Science Graduate Fellowship Program (DOE SCGF), made possible in part by the American Recovery and Reinvestment Act of 2009, administered by ORISE-ORAU under Contract No. DE-AC05-06OR23100. M.B.-F. and A.A.-G. acknowledge support from the US Department of Energy through Grant No. DE-SC0008733 and the Global Climate and Energy Project (Stanford Grant No. 25591130-45282-A). J.X. and G.X. acknowledge National Science Foundation of China (NSFC 51133002) for funding. J.R. acknowledges support by the Swedish Knut and Alice Wallenberg Foundation. This work is partly supported by the German Research Foundation (DFG) within the Cluster of Excellenc e 'Center for Advancing Electronics Dresden'.

■ REFERENCES

(1) Giri, G.; Verploegen, E.; Mannsfeld, S. C. B.; Atahan-Evrenk, S.; Kim, D. H.; Lee, S. Y.; Becerril, H. A.; Aspuru-Guzik, A.; Toney, M. F.; Bao, Z. A. *Nature* **2011**, *480*, 504.
(2) Diao, Y.; Tee, B. C. K.; Giri, G.; Xu, J.; Kim, D. H.; Becerril, H. A.; Stoltenberg, R. M.; Lee, T. H.; Xue, G.; Mannsfeld, S. C. B.; Bao, Z. N. *Nat. Mater.* **2013**, *12*, 665.
(3) Achar, B. N.; Lokesh, K. S. *J. Solid State Chem.* **2004**, *177*, 1987.
(4) Poelking, C.; Andrienko, D. *Macromolecules* **2013**, *46*, 8941.

(5) Chen, J.; Anthony, J.; Martin, D. C. *J. Phys. Chem. B* **2006**, *110*, 16397.
(6) Horowitz, G.; Bachet, B.; Yassar, A.; Lang, P.; Demanze, F.; Fave, J.-L.; Garnier, F. *Chem. Mater.* **1995**, *7*, 1337.
(7) Käfer, D.; El Helou, M.; Gemel, C.; Witte, G. *Cryst. Growth Des.* **2008**, *8*, 3053.
(8) Troisi, A.; Orlandi, G. *J. Phys. Chem. B* **2005**, *109*, 1849.
(9) Käfer, D.; Ruppel, L.; Witte, G.; Wöll, C. *Phys. Rev. Lett.* **2005**, *95*, 166602.
(10) Jurchescu, O. D.; Mourey, D. A.; Subramanian, S.; Parkin, S. R.; Vogel, B. M.; Anthony, J. E.; Jackson, T. N.; Gundlach, D. J. *Phys. Rev. B: Condens. Matter Mater. Phys.* **2009**, *80*, 085201.
(11) Yuan, Y.; Giri, G.; Ayzner, A. L.; Zoombelt, A. P.; Mannsfeld, S. C. B.; Chen, J.; Nordlund, D.; Toney, M. F.; Huang, J.; Bao, Z. *Nat. Commun.* **2014**, *5*, 3005.
(12) Cheng, H.-L.; Mai, Y.-S.; Chou, W.-Y.; Chang, L.-R.; Liang, X.-W. *Adv. Funct. Mater.* **2007**, *17*, 3639.
(13) Mannsfeld, S. C. B.; Virkar, A.; Reese, C.; Toney, M. F.; Bao, Z. *Adv. Mater.* **2009**, *21*, 2294.
(14) Yang, H.; Shin, T. J.; Ling, M.-M.; Cho, K.; Ryu, C. Y.; Bao, Z. *J. Am. Chem. Soc.* **2005**, *127*, 11542.
(15) Yuan, G.-C.; Lu, Z.; Xu, Z.; Gong, C.; Song, Q.-L.; Zhao, S.-L.; Zhang, F.-J.; Xu, N.; Gan, Y.; Yang, H.-B.; Li, C. M. *Org. Electron.* **2009**, *10*, 1388.
(16) Virkar, A.; Mannsfeld, S.; Oh, J. H.; Toney, M. F.; Tan, Y. H.; Liu, G.-y.; Scott, J. C.; Miller, R.; Bao, Z. *Adv. Funt. Mater.* **2009**, *19*, 1962.
(17) Kim, D. H.; Lee, H. S.; Yang, H.; Yang, L.; Cho, K. *Adv. Funct. Mater.* **2008**, *18*, 1363.
(18) Cheng, H.-L.; Lin, J.-W. *Cryst. Growth Des.* **2010**, *10*, 4501.
(19) Wedl, B.; Resel, R.; Leising, G.; Kunert, B.; Salzmann, I.; Oehzelt, M.; Koch, N.; Vollmer, A.; Duhm, S.; Werzer, O.; Gbabode, G.; Sferrazza, M.; Geerts, Y. *RSC Adv.* **2012**, *2*, 4404.
(20) Diao, Y.; Shaw, L.; Bao, Z.; Mannsfeld, S. C. B. *Energy Environ. Sci.* **2014**, *7*, 2145.
(21) Anthony, J. E.; Brooks, J. S.; Eaton, D. L.; Parkin, S. R. *J. Am. Chem. Soc.* **2001**, *123*, 9482.
(22) Le Berre, M.; Chen, Y.; Baigl, D. *Langmuir* **2009**, *25*, 2554.
(23) McMillan, P. F.; Wilson, M.; Daisenberger, D.; Machon, D. *Nat. Mater.* **2005**, *4*, 680.
(24) Hugo, K. C. *J. Phys.: Condens. Matter* **2001**, *13*, R95.
(25) James, R. D. *J. Mech. Phys. Solids* **1986**, *34*, 359.
(26) Mannsfeld, S. C. B.; Tang, M. L.; Bao, Z. *Adv. Mater.* **2011**, *23*, 127.
(27) *Avogadro—Free Cross-Platform Molecule Editor*. http://avogadro.openmolecules.net/wiki/Main_Page, accessed January 18, 2014.
(28) *TINKER Molecular Modeling*. http://dasher.wustl.edu/tinker/, accessed January 18, 2014.
(29) Allinger, N. L.; Yuh, Y. H.; Lii, J. H. *J. Am. Chem. Soc.* **1989**, *111*, 8551.
(30) Studies conducted by Prof. Peter Frazier, S. o. O. R. I. E., Cornell University. Private communication (2014).
(31) Charbonneau, P.; Kurchan, J.; Parisi, G.; Urbani, P.; Zamponi, F. *Nat. Commun.* **2014**, *5*, 3725.
(32) Brown, K. S.; Hill, C. C.; Calero, G. A.; Myers, C. R.; Lee, K. H.; Sethna, J. P.; Cerione, R. A. *Phys. Biol.* **2004**, *1*, 184.
(33) Gutenkunst, R. N.; Waterfall, J. J.; Casey, F. P.; Brown, K. S.; Myers, C. R.; Sethna, J. P. *PLoS Comput. Biol.* **2007**, *3*, 1871.
(34) Machta, B. B.; Chachra, R.; Transtrum, M. K.; Sethna, J. P. *Science* **2013**, *342*, 604.
(35) Arago, J.; Viruela, P. M.; Orti, E.; Malave Osuna, R.; Hernandez, V.; Lopez Navarrete, J. T.; Swartz, C. R.; Anthony, J. E. *Theor. Chem. Acc.* **2011**, *128*, 521.
(36) Xu, J.; Diao, Y.; Zhou, D.; Mao, Y.; Giri, G.; Chen, W.; Liu, N.; Mannsfeld, S. C. B.; Xue, G.; Bao, Z. *J. Mater. Chem. C* **2014**, *2*, 2985.
(37) Li, H.; Tee, B. C. K.; Giri, G.; Chung, J. W.; Lee, S. Y.; Bao, Z. *Adv. Mater.* **2012**, *24*, 2588.
(38) Naab, B. D.; Himmelberger, S.; Diao, Y.; Vandewal, K.; Wei, P.; Lussem, B.; Salleo, A.; Bao, Z. *Adv. Mater.* **2013**, *25*, 4663.
(39) Siegrist, T.; Besnard, C.; Haas, S.; Schiltz, M.; Pattison, P.; Chernyshov, D.; Batlogg, B.; Kloc, C. *Adv. Mater.* **2007**, *19*, 2079.
(40) Mannsfeld, S. C. B.; Fritz, T. *Phys. Rev. B: Condens. Matter Mater. Phys.* **2005**, *71*, 235405.
(41) Becke, A. D. *J. Chem. Phys.* **1993**, *98*, 5648.
(42) Stephens, P. J.; Devlin, F. J.; Chabalowski, C. F.; Frisch, M. J. *J. Phys. Chem.* **1994**, *98*, 11623.
(43) Harihara, Pc; Pople, J. A. *Theor. Chim. Acta* **1973**, *28*, 213.
(44) Kirkpatrick, J. *Int. J. Quantum Chem.* **2008**, *108*, 51.
(45) Neese, F. *Wiley Interdiscip. Rev.: Comput. Mol. Sci.* **2012**, *2*, 73.